ResearchGate

See discussions, stats, and author profiles for this publication at: https://www.researchgate.net/publication/231642502

Triple-Crystal Zinc Selenide Nanobelts

ARTICLE *in* THE JOURNAL OF PHYSICAL CHEMISTRY C · JUNE 2007

Impact Factor: 4.77 · DOI: 10.1021/jp0704160

CITATIONS
22

READS
10

7 AUTHORS, INCLUDING:

Shuangyi Liu
Chongqing Institute of Green and Intelligent …
32 PUBLICATIONS **152** CITATIONS
SEE PROFILE

Lei Jin
Forschungszentrum Jülich
26 PUBLICATIONS **252** CITATIONS
SEE PROFILE

Y. P. Leung
The University of Hong Kong
19 PUBLICATIONS **427** CITATIONS
SEE PROFILE

A. K. Soh
Monash University (Malaysia)
97 PUBLICATIONS **1,005** CITATIONS
SEE PROFILE

Available from: A. K. Soh
Retrieved on: 30 January 2016

Triple-Crystal Zinc Selenide Nanobelts

S. Y. Liu,[†,‡] Wallace C. H. Choy,*[,†] L. Jin,[†,§] Y. P. Leung,[†] G. P. Zheng,[‡] Jianbo Wang,[§] and A. K. Soh[‡]

Department of Electrical and Electronic Engineering, Department of Mechnical Engineering, University of Hong Kong, Pokfulam Road, Hong Kong, and Department of Physics and Center for Electron Microscopy, Wuhan University, Wuhan, 430072, China

Received: January 17, 2007; In Final Form: April 21, 2007

One-dimensional ZnSe nanobelts with three-dimensional triple-crystal architecture have been fabricated on Au-coated Si substrates by thermal evaporation of ZnSe powders. The as-synthesized triple-crystal ZnSe nanobelts are a metastable 2H-wurtzite structure while the typical structure of ZnSe nanocrystal is a stable zinc blend. The triple-crystal nanobelts have a typical length of tens of micrometers and a thickness of 30−80 nm. The morphology and growth mechanisms of the triple-crystal nanobelts, which cannot be described by the commonly used octahedral multiple-twin growth model for similar nanostructures, are investigated and explained based on the $\{10\bar{1}3\}$ twins and two fastest-growing directions of [0001] and $[1\bar{1}00]$ of the belt. The thermodynamics of the formation of metastable wurtzite ZnSe nanostructures are also discussed in terms of the temperature and surface energy. The photoluminescence spectra show that the triple-crystal nanobelts possess high-quality crystalline structure.

1. Introduction

Recently, many papers have reported on II−VI compound semiconductor nanomaterials with wurtzite structure, particularly in ZnO and ZnS, because of their interesting properties such as piezoelectricity and pyroelectricity resulting from the noncentrosymmetric wurtzite structure. These low-dimensional II−VI compounds show tremendous potential in engineering applications.[1] For example, one-dimensional (1D) wurtzite ZnO nanowires can be used as the main component of a nanogenerator to power nanoscale devices.[2] It has been demonstrated that the shape, morphology, and structural parameters have significant influence on the properties of nanostructures.[3,4] For some sophisticated nanocrystals, such as three-terminal ballistic junctions or Y-branch junctions,[5,6] novel properties or applications might emerge. To date, the control of shape and morphology of these nanostructures mainly rely on the anisotropic nucleation and growth of the nanocrystal from the liquid phase. There are other typical methods to control the shape and morphology of the nanostructures such as the regulation of the growth rates of different crystal facets and growth on templates.[7,8] In the synthesis of 1D nanocrystals, observation of the growth of three-dimensional (3D) architecture is very rare.[9,10]

Because of its wide band gap, ZnSe is a promising material for the fabrication of various optoelectronic devices such as solar cells, light-emitting diodes, and lasers that operate in the blue-green color region and near-infrared (NIR) window optics.[11−13] Given the abovementioned unique properties of those materials with wurtzite structure, ZnSe nanocrystals may have more applications in industry. Because of the thermodynamically unstable wurtzite phase of ZnSe at ambient conditions,[14] most of the reported ZnSe nanomaterials have zinc-blend structure.[15] Detailed description and explanation of its wurtzite counterpart are very limited.[16] For the wurtzite 1D ZnSe nanostructures with 3D architectures, there is only one report of ZnSe tetrapods by Hu.[17]

In this paper, we report the synthesis of controllable and repeatable growth of 3D wurtzite ZnSe triple-crystal nanobelts (TCNBs) with sawlike shape of each belt using thermal evaporation. The morphology of as-synthesized samples is discussed in Section 3.1. The crystal structure of TCNBs is characterized and determined to be 2H-wurtzite structure, and the angles between adjacent belts of TCNBs are determined. The formation of sawlike shape and 3D architecture is explained in detail in Section 3.2. In Section 3.3, the formation mechanism of the thermodynamically unstable wurtzite phase is discussed. Photoluminescence (PL) of TCNBs at 10 K is investigated in Section 3.4. The summary is given in Section 4.

2. Experimental Section

The TCNBs were grown in a two-zone tube furnace. ZnSe powder of about 0.5 g (99.99% Sigma Aldrich) was placed in an alumina boat, and the boat was then loaded into the first zone monitored by a thermocouple. Cleaned Si (100) substrates coated with 5 nm thick Au was placed in the downstream second zone monitored by another thermocouple. The system was then evacuated for 60 min and purged with the carrier gas (95% Ar + 5% H_2) at a rate of 200 sccm (sccm denotes cubic centimeter per minute at standard temperature and pressure) for 1 h to remove residual oxygen. The flow of the carrier gas was then kept at 400 sccm throughout the growth. The first zone was then heated up to 1000 °C and was maintained at the temperature for 40 min. A different temperature was maintained for 50 min in the second zone to synthesize the nanostructures. The pressure was kept at 100 Torr. After growth, the system was cooled gradually to room temperature. Some yellow-colored products

* To whom correspondence should be addressed. Email: chchoy@eee.hku.hk. Phone: (852) 2857-848. Fax: (852) 2558-8738.

[†] Department of Electrical and Electronic Engineering, University of Hong Kong.

[‡] Department of Mechnical Engineering, University of Hong Kong.

[§] Department of Physics and Center for Electron Microscopy, Wuhan University.

10.1021/jp0704160 CCC: $37.00 © 2007 American Chemical Society
Published on Web 06/07/2007

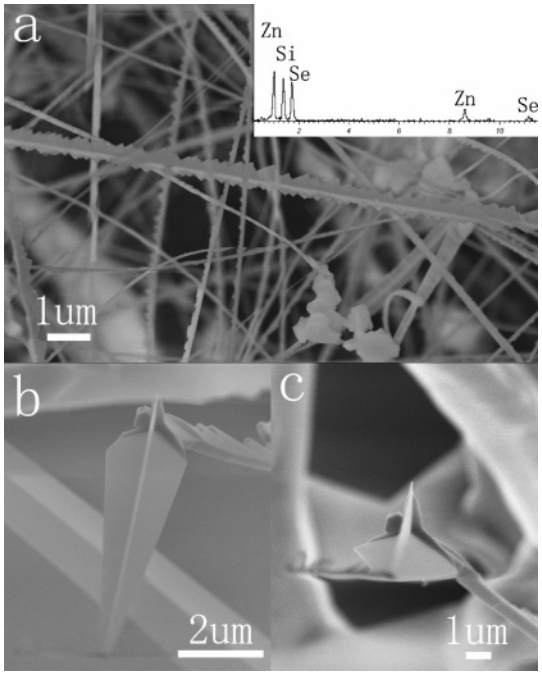

Figure 1. SEM image of ZnSe TCNBs. (a) Low-magnification image inserted with EDX of TCNBs. (b−c) Enlarged images from different viewing angle.

were obtained on the Si substrates after the growth when the temperature of the second zone was set at the range of 750−850 °C.

The as-synthesized samples were characterized by field emission scanning electron microscopy (FE-SEM, LEO 1530) equipped with an energy dispersive X-ray spectroscopy (EDX), field emission transmission electron microscopy (TEM, JEOL-2010F) equipped with an EDX, and PL system with a temperature controllable cryostat from 300 to 10 K. For SEM observations, the Si substrate with as-synthesized products was fixed on the holder of the SEM using conductive adhesive. The specimens for TEM and high-resolution TEM (HRTEM) were prepared by dispersing the as-synthesized products in ethanol and immersing them in an ultrasonic bath for 2 min, then dropping a few drops of the resulting suspension containing the synthesized materials onto a Cu grid coated with a holey carbon.

3. Results and Discussion

3.1. Morphology of TCNBs. Figure 1a shows the SEM image of as-synthesized nanostructures with the sawlike shape grown at the substrate temperature of 800 °C. It reveals that the products are not the common 1D nanostructures such as rods, wires, belts, and ribbons, but a complex 3D architecture of triple-crystal nanobelts with a length of tens of micrometers. Figure 1b,c shows the SEM images from different viewing angles and larger magnifications. The images show that the TCNBs consist of three intersecting belts sharing a common spine, and each belt of the TCNBs has the thickness of less than 80 nm. The EDX spectrum of the inset of Figure 1a shows that the TCNBs are composed only of Zn and Se with a ratio of about 1:1. The Si peak comes from the Si substrate.

The details of the nanostructures are investigated by using TEM, selected-area electron diffraction (SAED), and HRTEM. The bright-field TEM image of a TCNB is shown in Figure 2a. The similar SAED patterns and HRTEM images that were taken randomly from the belts of single TCNBs or belts of different

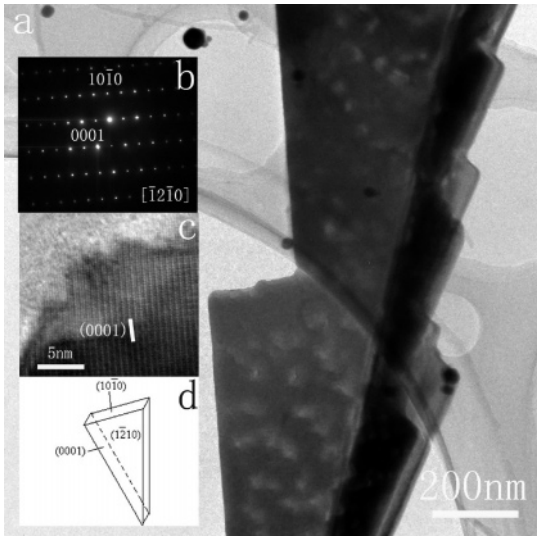

Figure 2. (a) Bright-field TEM image of ZnSe TCNBs. (b) SAED pattern of one sawtooth. (c) HRTEM image. (d) Sketch diagram of one sawtooth.

TCNBs as shown in Figure 2b,c were attained. Figure 2b,c is SAED patterns and the HRTEM image taken from one belt of TCNBs, as shown in the Figure 2a. It is confirmed that the nanostructure is 2H-wurtzite ZnSe, and each saw structure has the facet planes of (0001), $(10\bar{1}0)$, and $(11\bar{2}0)$ as indicated in the schematic illustration of Figure 2d. To obtain further structural information on the TCNBs, the nanostructures are analyzed in detail by a series of tilted TEM images at various viewing angles. The SAED pattern of Figure 3b taken around the TCNBs spine, as shown in Figure 3a, shows two sets of diffraction patterns having a twin relationship with a common spine plane, and each set can be indexed with the $[\bar{1}3\bar{2}1]$ axis. Figure 3c is an HRTEM image corresponding to Figure 3a. It can be observed that the spine is straight and uniform, and the angle between the (0001) plane and spine is determined to be 18° as shown in the image. The spine is confirmed to be along the direction of $[3\bar{3}01]$, and the plane in which the spine locates is $(0\bar{1}13)$, which corresponds to the twin plane.

Figure 3d is a dark-field image of a typical TCNB. The diffraction pattern of the three belts of the TCNBs in Figure 3d is shown in Figure 3e. From the diffraction pattern, the three angles between any two adjacent branches can be determined. A tetrahedron model is constructed on the dark-field image of TCNBs in Figure 3d, which shows the principle of the calculation. Line 1 and line 2 with the same length denote the [0001] direction of belt A and belt B of the TCNBs. Line 3 denotes the spine and line 4 denotes the edge of the sawtooth as shown in Figure 3d. The other two lines used to form the tetrahedron diagram are normal lines of the spine. In the tetrahedron model, angle δ is the included angle of belt A and belt B. Meanwhile, angle α equals to angle β, which are the angles between the [0001] plane and the spine. Angle γ can be obtained through calculating the included angle between the [0001] direction of belt A (line 1) and [0001] direction of belt B (line 2). The [0001] direction of belt A is parallel to $[\bar{3}5\bar{2}1]$ direction of belt B, as shown in Figure 3e. The angle δ can be calculated based on the relationship of angles in the tetrahedron model, and the result is about 117°. The remaining two angles between three belts of TCNBs can be obtained using the same method. When the error in TEM measurement and analysis is taken into account, the three angles between every two adjacent belts are confirmed to be 117, 117, and 126°. The angles are

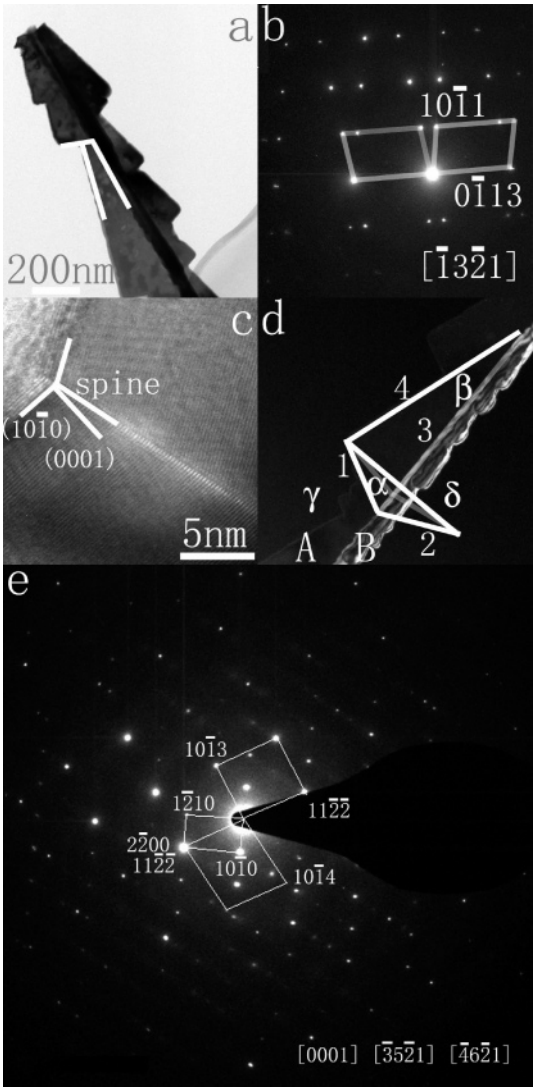

Figure 3. (a) Bright-field TEM image of ZnSe TCNBs. (b) SAED pattern around spine of TCNBs shown in (a). (c) HRTEM image of TCNBs corresponding to the TCNBs shown in (a). (d) Dark-field TEM image of ZnSe TCNBs and SAED pattern shown in (e), and tetrahedron model for calculating the angle between two belts: $\sin \delta/2 = \sin \gamma/2/\cos \alpha$, (e) SAED pattern including three sets of spots.

very useful for investigating the growth mechanism of the as-synthesized products.

3.2. Formation of the TCNBs. In our experiments, Au particles are found on the top of TCNBs, as shown in Figure 4, revealing that the TCNBs grow based on the VLS mechanism.[18] The growth direction of TCNBs is different from the growth directions of typical 1D ZnSe nanostructures, which have been reported based on the VLS growth mechanism. However, the growth direction of the TCNBs can be dissociated to become $[3\bar{3}01] = [0001] + 3[1\bar{1}00]$. Our study[19] for the surface energy of wurtzite ZnSe nanostructures suggested that the energy of {0001} facet is the highest followed by $\{1\bar{1}00\}$ and $\{2\bar{1}10\}$. As a result, [0001] and $[1\bar{1}00]$ are the fastest growing directions, while $\{2\bar{1}\bar{1}0\}$ becomes the dominant surface of the ZnSe nanostructures, as shown in Figure 2d. Meanwhile, the multiple factor of 3 of $[1\bar{1}00]$ reveals that growth rate along the $[1\bar{1}00]$ direction may probably be faster than that along [0001] direction. Hence the formation of the sawlike shape of TCNBs can be well understood through the two-directional growth, as shown in Figure 5d.

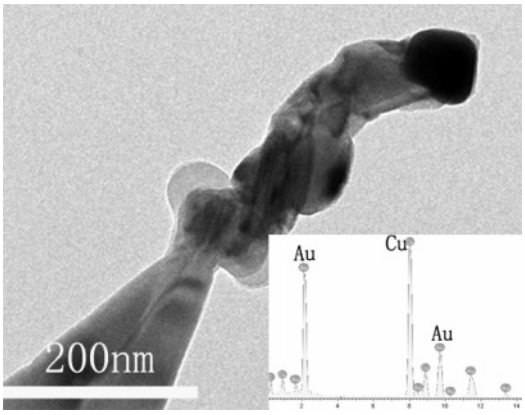

Figure 4. Bright-field TEM image of TCNBs with a catalyst grain and EDX spectrum.

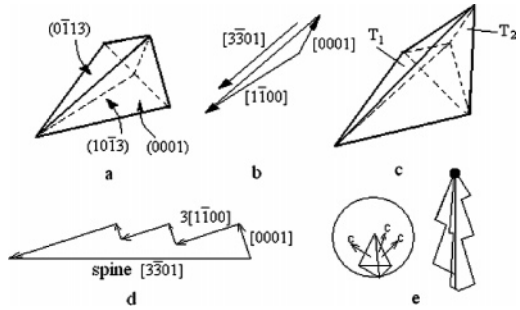

Figure 5. Sketch of the growth mechanism of ZnSe TCNBs.

It is reported that dart-shaped tricrystal ZnS nanoribbons,[9] which also show tricrystal structure but different geometry details to our products, form the 3D structure based on the octahedral multiple-twin growth model. The growth model has also been used successfully to explain the tetrapod ZnO and ZnSe.[20,21] However, the octahedral multiple-twin growth model cannot explain well the formation of our products, particularly the explanation of the plane of the twin, the grow direction of the belt, and the angles between any two adjacent belts. In other words, the octahedron model based on $\{11\bar{2}2\}$ twins cannot construct the 3D architecture of our TCNBs properly, and we are not able to find the $\{11\bar{2}2\}$ twin planes in any of our studied samples. According to our HRTEM and SAED results, the twin of our TCNBs has the common spine plane of $(0\bar{1}13)$, which are the most frequently observed twin structures of wurtzite ZnO and CdSe twin belts fabricated by controlling the deposition conditions,[22] and it agrees with the model prediction that the $\{10\bar{1}3\}$ twins may have the lowest energy for wurtzite structures and that the six-coordinated channels minimize the distortion of the tetracoordination.[23] Hence, we propose that the growth mechanism of TCNBs is based on both polarity and twin growth. Figure 5a illustrates the initial nucleus. Its surfaces consist of (0001), $(10\bar{1}3)$, and $(0\bar{1}13)$, and the intersection of $(10\bar{1}3)$ and $(0\bar{1}13)$ is along $[3\bar{3}01]$ direction. As shown in Figure 5c, T_1 and T_2 are primary twinned crystals based on $\{10\bar{1}3\}$ planes forming the pyramidal crystal with three polarity (0001) planes. The intersection of two primary twinned crystals (T_1 and T_2) and the initial crystal is just along the $[3\bar{3}01]$ direction. Therefore, in the initial growth stage, it is considered that a pyramidal crystal forms at the molten gold catalyst. It then grows along three *c*-axes and the spine direction, and this will lead to the formation of TCNBs shown in Figure 5e. The angle between the $(10\bar{1}3)$ plane and the $(01\bar{1}3)$ plane is about 54°. Thus, the angle between the belts grown based on the $(10\bar{1}3)$ plane and the $(10\bar{1}3)$ plane is 126°. The angles between (0001) and (0001)

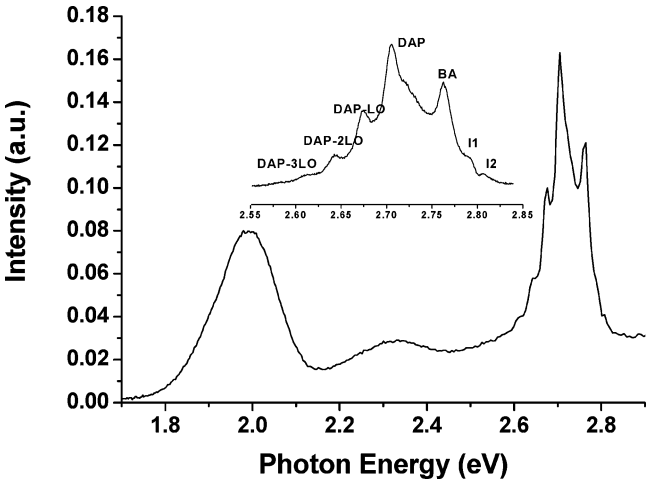

Figure 6. Photoluminescent spectrum of as-synthesized ZnSe TCNBs at 10 K.

of two primary twins are 117°. The angles coincide with our results discussed in Section 2.2 about the angles between each two belts of TCNBs. Consequently, the growth of the $\{10\bar{1}3\}$ twin and along the two fastest-growing directions of [0001] and $[1\bar{1}00]$ of each belt of TCNBs forms the sawlike shape and 3D architecture of the as-synthesized samples.

3.3. Thermodynamic Growth Mechanism. For the formation of the thermodynamically unstable wurtzite ZnSe nanostructures, the growth temperature and surface energy are two important factors. A series of experiments have been conducted to study the influence of temperature on the crystalline structures. We find that the wurtzite phase becomes the dominant phase when the growth temperature is higher than 700 °C. It should be noted that in bulk ZnSe, the zinc-blend structure transforms into the wurtzite structure when the temperature is above the transition temperature (T_{tr}) of 1411 °C.[24] However, when the particle size reduces, T_{tr} will significantly reduce.[25] In our case, wurtzite ZnSe nanostructures form when the substrate temperature is above 700 °C.

It is worth noting that the transformation from wurtzite structure to zinc-blend structure will occur by cooling.[24] However, our wurtzite-phase ZnSe TCNBs are maintained when the temperature of the sample is reduced to room temperature. On the basis of our study of the surface energy of ZnSe,[19] it can be deduced that nonpolar $\{2\bar{1}\bar{1}0\}$ planes have the lowest energy as compared with other planes of the wurtzite structure. Meanwhile, their energy is also lower than the lowest surface energy plane of {110} of zinc-blend phase. Because the dominant plane of our products is $\{2\bar{1}\bar{1}0\}$, as shown in Figure 2d, the total surface energy will be minimized. Thus, the wurtzite-phase ZnSe TCNBs are obtained at room temperature.

3.4. PL of the ZnSe TCNBs. The PL spectrum of the wurtzite tricrystal nanobelts at 10 K is shown in Figure 6, and the inset spectrum of Figure 6 is the fine scanning PL spectrum at 10 K. The emission peaks of ~2.806 and ~2.792 eV (I_2 and I_1) are attributed to bound excitons and free exciton, respectively, and the peak of ~2.762 eV is attributed to band-to-acceptor transition.[26,27] At energies of 2.705, 2.675, 2.645, and 2.615 eV, donor−acceptor-pair (DAP) and longitudinal optical phonon replicas with a phonon energy around 30 meV are obtained. The peak of 2.3−2.4 eV shows a unique broad green band of the samples, which are likely associated with the vacancies of Zn in ZnSe.[28,29] Because emission peaks of the exciton and DAP state transitions can be clearly resolved in our PL spectra, it is considered that the TCNBs possess high-crystalline quality. It is interesting to note that a simple physical evaporation is used in our experiment to achieve the high-quality ZnSe nanostructures whereas such high-quality ZnSe nanostructures are typically only reported using sophisticated evaporation systems of metal−organic chemical vapor deposition and molecular-beam epitaxy.[26,28]

4. Summary

In conclusion, 3D triple-crystal ZnSe nanobelts have been synthesized by thermal evaporation. The TCNBs have a 2H-wurtzite structure and show a 3D morphology in which three intersecting belts share a common spine. The as-synthesized ZnSe belts have lengths of tens of micrometers, and the thickness of each belt, which has a sawlike shape, is about 30−80 nm. The morphology and growth mechanism of TCNBs are explained based on the two fastest growing directions of [0001] and $[1\bar{1}00]$ for the 1D belts with 2H-wurtzite structure and $\{10\bar{1}3\}$ twins. We conclude that the thermodynamically unstable wurtzite phase can be eventually obtained at room temperature because the growth temperature is higher than T_{tr}, and the dominant nonpolar $\{2\bar{1}\bar{1}0\}$ surfaces of our products have the lowest surface energy in both wurtzite phase and zinc-blend phase. The PL spectrum of TCNBs shows clear bound emission and DAP peaks, which reveals that the nanostructures possess high-crystalline quality.

Acknowledgment. This work was supported by the University Development Fund (UDF) and the seed funding (200411159137) of the University of Hong Kong and Competitive Earmarked Research Grant (CERG), Project No. HKU 7124/05E from the Research Grants Council of the Hong Kong Special Administrative Region, China. G.P.Z. thanks the support of CERG, Project No. HKU 7200/05E. S.Y.L. acknowledges the financial support of HKU 7124/05E and HKU 7200/05E. We acknowledge the help of Andrew W.O. Poon and his group for part of the TEM characterization in the MCPF facilities at the Hong Kong University of Science and Technology.

References and Notes

(1) Law, M.; Goldberger, J.; Yang, p. *Annu. Rev. Mater. Res.* **2004**, *34*, 83.
(2) Wang, Z. L.; Song, J. H. *Science* **2006**, *312*, 242.
(3) Alivisatos, A. P. *Science* **1996**, *271*, 933.
(4) Lieber, C. M. *Solid State Commun.* **1998**, *107*, 607.
(5) Hieke, K.; Ulfward, M. *Phys. Rev. B* **2000**, *62*, 16727.
(6) Rashmi Bednarz, L.; Hackens, B.; Farhi, G.; Bayot, V.; Huynen, I. *Solid State Commun.* **2005**, *134*, 217.
(7) Tanori, J.; Pileni, M. P. *Langmuir* **1997**, *13*, 639.
(8) Li, M.; Schnablegger, H.; Mann, S. *Nature* **1999**, *402*, 393.
(9) Fan, X.; Meng, X. M.; Zhang, X. H.; Shi, W. S.; Zhang, W. J.; Zapien, J. A.; Lee, C. S.; Lee, S. T. *Angew. Chem., Int. Ed.* **2006**, *45*, 2568.
(10) (a) Manna, L.; Scher, E. C.; Alivisatos, A. P. *J. Am. Chem. Soc.* **2000**, *122*, 12700. () Manna, L.; Milliron, D. J.; Meisel, A.; Scher, E. C.; Alivisatos, A. P. *Nat. Mater.* **2003**, *2*, 382.
(11) Matasuoka, T. *Adv. Mater.* **1996**, *8*, 469.
(12) Passler, R.; Griebl, E.; Ripel, H.; Lautner, G.; Bauer, S.; Preis, H; Gebhardt, W.; Buda, B.; As D. J.; Schikora, D.; Lischka, K.; Papagelis, K.; Ves, S. *J. Appl. Phys.* **1999**, *86*, 4403.
(13) Wang, J.; Hutchings, D. C.; Miller, A.; Vanstryland, E. W.; Welford, K. R.; Muirhead, I. T.; Lewis, K. L. *J. Appl. Phys.* **1993**, *73*, 4746.
(14) Yeh, C. Y.; Lu, Z. W.; Froyen, S.; Zunger, A. *Phys. Rev. B* **1992**, *46*, 10086.
(15) (a) Choy, W. C. H.; Guo, C. F.; Leung, Y. P.; Wang, G. Z.; Yuk, T. I. *Appl. Phys. A* **2006**, *83*, 301. (b) Zhu, Y. C.; Bando, Y. *Chem. Phys. Lett.* **2003**, *377*, 367.
(16) Leung, Y. P.; Choy, W. C. H.; Markov, I.; Pang, G. K. H.; Ong, H. C.; Yuk, T. I. *Appl. Phys.* **2006**, *88*, 183110.
(17) Hu, J. Q.; Bando, Y.; Golberg, D. *Small* **2005**, *1*, 95.

(18) Wagner, R. S.; Ellis, W. C. *Appl. Phys. Lett.* **1964**, *4*, 89.

(19) Jin, L.; Choy, W. C. H.; Leung, Y. P.; Yuk, T. I.; Ong, H. C.; Wang, J. *J. Appl. Phys.*, submitted for publication.

(20) (a) Fuller, M. L. *J. Appl. Phys.* **1943**, *15*, 164. (b) Djurišić, A. B.; Choy, W. C. H.; Roy, V. A. L.; Leung, Y. H.; Kwong, C. Y.; Cheah, K. W.; Gundu, R. T. K.; Chan, W. K.; Lui, H. F.; Surya, C. *Adv. Funct. Mater.* **2004**, *14*, 856.

(21) Iwanaga, H.; Fujii, M.; Takeuchi, S. *J. Cryst. Growth* **1993**, *134*, 275.

(22) Ding, Y.; Wang, Z. L. *J. Phys. Chem. B* **2004**, *108*, 12280.

(23) Be're', A.; Serra, A. *Phys. Rev. B.* **2003**, *68*, 033305.

(24) Okada, H.; Kawanaka, T.; Ohmoto, S. *J. Cryst. Growth* **1996**, *165*, 31.

(25) Qadri, S. B.; Skelton, E. F.; Hsu, D.; Dinsmore, A. D.; Yang, J.; Gray, H. F.; Ratna, B. R. *Phys. Rev. B* **1999**, *60*, 9191.

(26) Zhang, X. T.; Ip, K. M.; Liu, Z.; Leung, Y. P.; Li, Q.; Hark, S. K. *Appl. Phys. Lett.* **2004**, *84*, 2641.

(27) Gutowski, J.; Presser, N.; Kudlek, G. *Phys. Status Solidi* **1990**, *120*, 11.

(28) Cilli, A.; Martelli, F.; Rubini, S.; Ducati, C.; Hofmann, S.; Ferrari A. C.; Robertson J.; Franciosi A. 4th IEEE Conference on Nanotechnology, Munich, Germany, Aug 16−19, 2004.

(29) Fujita, S.; Mimoto, H.; Naguchi, T. *J. Appl. Phys.* **1979**, *50*, 1079.